

This work was written as part of one of the author's official duties as an Employee of the United States Government and is therefore a work of the United States Government. In accordance with 17 U.S.C. 105, no copyright protection is available for such works under U.S. Law. Access to this work was provided by the University of Maryland, Baltimore County (UMBC) ScholarWorks@UMBC digital repository on the Maryland Shared Open Access (MD-SOAR) platform.

Please provide feedback

Please support the ScholarWorks@UMBC repository by emailing scholarworks-group@umbc.edu and telling us what having access to this work means to you and why it's important to you. Thank you.

Second harmonic generation from metallo-dielectric multilayered structures in the plasmonic regime

Nadia Mattiucci,^{1,2,*} Giuseppe D'Aguanno,^{1,2} and Mark J. Bloemer¹

¹C. M. Bowden Facility, Bldg 7804, RDECOM, Redstone Arsenal AL35898, USA

²Aegis Technologies Group, 410 Jan Davis Drive, Huntsville AL 35806, USA

*nadia.mattiucci@us.army.mil

Abstract: We present a theoretical study on second harmonic generation from metallo-dielectric multilayered structures in the plasmonic regime. In particular we analyze the behavior of structures made of Ag (silver) and MgF₂ (magnesium-fluoride) due to the straightforward procedure to grow these materials with standard sputtering or thermal evaporation techniques. A systematic study is performed which analyzes four different kinds of elementary cells- namely (Ag/MgF₂)^N, (MgF₂/Ag)^N, (Ag/MgF₂/Ag)^N and (MgF₂/Ag/MgF₂)^N-as function of the number of periods (N) and the thickness of the layers. We predict the conversion efficiency to be up to three orders of magnitude greater than the conversion efficiency found in the non-plasmonic regime and we point out the best geometries to achieve these conversion efficiencies. We also underline the role played by the short-range/long-range plasmons and leaky waves in the generation process. We perform a statistical study to demonstrate the robustness of the SH process in the plasmonic regime against the inevitable variations in the thickness of the layers. Finally, we show that a proper choice of the output medium can further improve the conversion efficiency reaching an enhancement of almost five orders of magnitude with respect to the non plasmonic regime.

©2010 Optical Society of America

OCIS codes: (190.0190) Nonlinear optics; (240.6680) Surface plasmons.

References and links

1. F. Brown, R. E. Parks, and A. M. Sleeper, "Nonlinear Optical Reflection from a Metallic Boundary," *Phys. Rev. Lett.* **14**(25), 1029–1031 (1965).
2. N. Bloembergen, R. K. Chang, S. S. Jha, and C. H. Lee, "Optical Second-Harmonic Generation in Reflection from Media with Inversion Symmetry," *Phys. Rev.* **174**(3), 813–822 (1968).
3. Y. R. Shen, *The Principles of Nonlinear Optics*, (Wiley, 1984)
4. H. J. Simon, D. E. Mitchell, and J. G. Watson, "Optical Second-Harmonic Generation with Surface Plasmons in Silver Films," *Phys. Rev. Lett.* **33**(26), 1531–1534 (1974).
5. E. Kretschmann, "The Determination of the Optical Constants of Metals by Excitation of Surface Plasmons," *Z. Phys.* **241**(4), 313–324 (1971).
6. J. C. Quail, and H. J. Simon, "Second-harmonic generation from silver and aluminum films in total internal reflection," *Phys. Rev. B Condens. Matter* **31**(8), 4900–4905 (1985).
7. T. Y. F. Tsang, "Surface-plasmon-enhanced third-harmonic generation in thin silver films," *Opt. Lett.* **21**(4), 245–247 (1996).
8. R. Naraoka, H. Okawa, K. Hashimoto, and K. Kajikawa, "Surface plasmon resonance enhanced second-harmonic generation in Kretschmann configuration," *Opt. Commun.* **248**(1-3), 249–256 (2005).
9. T. A. Leskova, M. Leyva-Lucero, E. R. Mendez, A. A. Maradudin, and I. V. Novikov, "The surface enhanced second harmonic generation of light from a randomly rough metal surface in the Kretschmann geometry," *Opt. Commun.* **183**(5-6), 529–545 (2000).
10. Q. Chen, X. Sun, I. R. Coddington, D. A. Goetz, and H. J. Simon, "Reflected second-harmonic generation with coupled surface-plasmon modes in Ag/liquid/Ag layers," *J. Opt. Soc. Am. B* **16**(6), 971–975 (1999).
11. J. G. Rako, J. C. Quail, and H. J. Simon, "Optical second-harmonic generation with surface plasmons in noncentrosymmetric crystals," *Phys. Rev. B* **30**(10), 5552–5559 (1984).
12. G. M. Wysin, H. J. Simon, and R. T. Deck, "Optical bistability with surface plasmons," *Opt. Lett.* **6**(1), 30–32 (1981).

13. M. Fukui, J. E. Sipe, V. C. Y. So, and G. I. Stegeman, "Nonlinear mixing of opposite traveling surface plasmons," *Solid State Commun.* **27**(12), 1265–1267 (1978).
14. C. K. Chen, A. R. B. de Castro, and Y. R. Shen, "Coherent second-harmonic generation by counterpropagating surface plasmons," *Opt. Lett.* **4**(12), 393–394 (1979).
15. H. A. Macleod, *Thin film optical filters*, (Institute of Physics Publishing, 2001)
16. N. Mattiucci, G. D'Aguanno, N. Akozbek, M. Scalora, and M. J. Bloemer, "Homogenization procedure for a metamaterial and local violation of the second principle of thermodynamics," *Opt. Commun.* **283**(8), 1613–1620 (2010).
17. T. Decoopman, G. Tayeb, S. Enoch, D. Maystre, and B. Gralak, "Photonic crystal lens: from negative refraction and negative index to negative permittivity and permeability," *Phys. Rev. Lett.* **97**(7), 073905 (2006).
18. *Handbook of Optical constants of solids*, E. D. Palik ed., (Academic Press Inc., 1991).
19. G. D'Aguanno, M. C. Larciprete, N. Mattiucci, A. Belardini, M. J. Bloemer, E. Fazio, O. Buganov, M. Centini, and C. Sibilia, "Experimental study of Bloch vector analysis in nonlinear, finite, dissipative systems," *Phys. Rev. A* **81**(1), 013834 (2010).
20. N. Mattiucci, G. D'Aguanno, M. J. Bloemer, and M. Scalora, "Second-harmonic generation from a positive-negative index material heterostructure," *Phys. Rev. E Stat. Nonlin. Soft Matter Phys.* **72**(6), 066612 (2005).
21. G. D'Aguanno, N. Mattiucci, M. Scalora, M. J. Bloemer, and A. M. Zheltikov, "Density of modes and tunneling times in finite one-dimensional photonic crystals: a comprehensive analysis," *Phys. Rev. E Stat. Nonlin. Soft Matter Phys.* **70**(1), 016612 (2004).
22. J. E. Sipe, V. C. Y. So, M. Fukui, and G. I. Stegeman, "Analysis of second-harmonic generation at metal surfaces," *Phys. Rev. B* **21**(10), 4389–4402 (1980).
23. M. Scalora, M. A. Vincenti, D. de Ceglia, V. Roppo, M. Centini, N. Akozbek, and M. J. Bloemer, "Second and Third Harmonic Generation in Metal-Based Nanostructures," at <http://arxiv.org/abs/1006.3841>
24. S. Ciraci, and I. P. Batra, "Theory of the quantum size effect in simple metals," *Phys. Rev. B Condens. Matter* **33**(6), 4294–4297 (1986).
25. H. Raether, "Surface Plasmons," *Springer Tracts in Modern Physics*, (Berlin, 1988)
26. D. Sarid, "Long-range surface-plasma waves on very thin metal films," *Phys. Rev. Lett.* **47**(26), 1927–1930 (1981).
27. N. Mattiucci, G. D'Aguanno, M. Scalora, M. J. Bloemer, and C. Sibilia, "Transmission function properties for multi-layered structures: application to super-resolution," *Opt. Express* **17**(20), 17517–17529 (2009).
28. G. D'Aguanno, M. Centini, M. Scalora, C. Sibilia, M. Bertolotti, M. J. Bloemer, and C. M. Bowden, "Generalized coupled-mode theory for $\chi^{(2)}$ interactions in finite multilayered structures," *J. Opt. Soc. Am. B* **19**(9), 2111 (2002).
29. J. J. Burke, G. I. Stegeman, and T. Tamir, "Surface-polariton-like waves guided by thin, lossy metal films," *Phys. Rev. B Condens. Matter* **33**(8), 5186–5201 (1986).

1. Introduction

Second harmonic generation (SHG) from metal surfaces in the non-plasmonic regime has been studied since the beginning of nonlinear optics [1,2] in the 60s. It is well known that metals possess both a volume and a surface quadratic nonlinearity [3]. The volume nonlinearity originates from the Lorentz force exerted on the free electrons of the metal, while the surface nonlinearity is due to the symmetry breaking at the metal surface [3]. The subject of plasmonic SHG was addressed just several years later in 1974 [4] when SH from a single layer of silver in the Kretschmann geometry [5] was studied both experimentally and theoretically. The work of Ref. [4] was then followed by several other works studying SHG in the Kretschmann configuration from smooth surfaces [6–8] and rough surfaces [9]. A more complex structure was analyzed in Ref. [10] where a thin layer of metal was grown on the base of a prism, then a second layer of metal was squeezed toward the prism with an index matching fluid in between. Besides the harmonic generation from the metal itself, plasmons have also been used to enhance nonlinear effects in an external medium [11,12]. The effect of counter-propagating plasmons has also been studied [13,14].

In this paper we analyze plasmonic SHG from metal/dielectric periodic stratifications. In particular we study SHG from structures made of Ag (silver) and MgF_2 (magnesium-fluoride) due to the simple procedure to grow these materials with standard sputtering or thermal evaporation techniques [15]. The paper is organized as follows: In Section 2 we describe in details the geometries studied and the model used in order to describe SHG. In Section 3 we discuss the conversion efficiencies achieved in these kinds of structures and the role played by the short-range/long-range plasmons and leaky waves in the generation process. We also perform a statistical study to investigate the robustness of the SH process in the plasmonic regime against the inevitable variations in the thickness of the layers. Finally in Section 4 we give our conclusions.

2. The model

Let us start our analysis by describing in Fig. 1 the types of geometries studied. A metal/dielectric one-dimensional (1-D) photonic crystal (PC) is grown on the flat side of a hemi-cylindrical prism. From a theoretical point of view we can assume with no loss of generality that the prism is the input medium with refractive index n_{in} and θ is the angle of the incident beam that is TM polarized. The total internal reflection condition will be achieved for incident angles so that $\theta > \text{asin}(n_{out}/n_{in})$ where $n_{out} < n_{in}$ and n_{out} is the refractive index of the output medium (air in our case). The above condition is satisfied for incident angles greater than 40.8° at 800nm incident wavelength. When total internal reflection is achieved, leaky waveguides modes can be excited. Those modes can either have a plasmonic or a non-plasmonic nature. In the first case plasmon-like modes are excited at each MgF_2/Ag interface or at the Ag/air interface when the termination of the structure is metallic. Plasmon excitation at the MgF_2/Ag interfaces is expected only for $\theta > \text{asin}(n_{\text{MgF}_2}/n_{in})$, i.e. $\theta > 63.5^\circ$, because at a single dielectric/metal interface the field must be evanescent in the semi-space occupied by the dielectric in order to be able to couple with the surface plasmon. In the framework of the total internal reflection condition we can distinguish two regimes: 1) the incident field is evanescent in the output medium but propagating in the dielectric layers ($40.8^\circ < \theta < 63.5^\circ$); 2) the incident field is evanescent both in the output medium and in the dielectric layers ($\theta > 63.5^\circ$). As we will see later, the passage from one regime to the other is actually characterized by a smooth transition with no abrupt changes. In other words, plasmon excitation at the various MgF_2/Ag interfaces is also responsible for the presence of leaky waveguide modes at angles of incidence $\theta < 63.5^\circ$. Those modes are just the natural evolution of “plasmonic” modes when the multilayer starts to manifest a collective response. We will exemplify this point later in the next Section with an example of these considerations. As we are studying finite structures, we also expect that the terminations of the PC are going to play a major role [16, 17]. For this reason, we study SH generation from periodic stratification, based on four different cuts of the elementary cell. The four types of stratification are as described in Fig. 1: symmetric-1, i.e. a symmetric structure that starts and ends with the dielectric [Fig. 1(a)]; asymmetric-1, i.e. an asymmetric structure that starts with the dielectric and ends with the metal [Fig. 1(b)]; asymmetric-2, i.e. an asymmetric structure that starts with the metal and ends with the dielectric [Fig. 1(c)]; and, symmetric-2, i.e. a symmetric structure that starts and ends with the metal [Fig. 1(d)]. All the simulations consider a fused silica prism (SiO_2) as input medium and Ag/MgF_2 stratifications while, the exit medium is air. All the refractive indexes used in the simulations have been taken from experimentally measured values available in the book of Palik [18].

The simulations are based on the theoretical model that we have developed in Ref. [19], where the non-plasmonic SHG from metallo-dielectric structures has been investigated both theoretically and experimentally. In Ref. [19] the quadratic nonlinearity of metals was described through two terms: the Lorentz term (volume term) and the surface term. In our case we can neglect the Lorentz term because in the plasmonic regime the field is mainly localized at the metal-dielectric interfaces and therefore just the surface term will be exploited in an efficient way. Under TM polarization, the Helmholtz equation for the H-field at the SH can be written as follows [19]:

$$\frac{d^2 H_{2\omega}}{dz^2} + \frac{4\omega^2}{c^2} (n_{2\omega}^2(z) - n_{in}^2 \sin^2 \theta) H_{2\omega} = \frac{4\omega^2 n_{in}}{c} \sin \theta \left(\epsilon_0 d_s^{(2)} \sum_k \delta(z - z_k) E_{z,\omega}^2 \right). \quad (1)$$

Equation (1) is valid layer by layer and describes the SH magnetic field generated from a TM polarized pump field, in a Cartesian, right-handed, reference system (x,y,z) where z is the direction of the stratification. Moreover, only the (z,z,z) component of the nonlinearities is considered, i.e. TM→TM SH emission. In Eq. (1), θ is the angle of incidence, n_{in} is the refractive index of the incident medium (the hemi-cylindrical prism made of fused silica in our case), $n_{2\omega}(z)$ is the step-varying, complex refractive index at the SH along the direction of

the stratification, $\varepsilon_0 \cong 8.85 \times 10^{-12}$ F/m is the vacuum permittivity, c is the speed of light in vacuo, $E_{z,\omega}$ is the z-component of the fundamental frequency (FF) electric field, $H_{2\omega}$ is the SH magnetic field, $\delta(z-z_k)$ is the Dirac “delta” function calculated at the k^{th} metal/dielectric interface just inside the metal and, finally, $d_s^{(2)}$ is the surface nonlinearity. The value of the surface nonlinearity is estimated to be $d_s^{(2)} = 10^{-18}$ m²/V, based on the experimental results reported Ref. [19]. In the undepleted regime, Eq. (1) can be solved using the Green function approach for multi-layered structures described in Ref. [20, 21]. and adapted here to handle TM polarization. The reader interested in the mathematical details of the theoretical approach can consult Ref. [19]. The SH conversion efficiency in reflection is calculated by the ratio of the z-component of the Poynting vector of the backward generated SH divided by the z-component of the Poynting vector of the FF pump field incident on the sample:

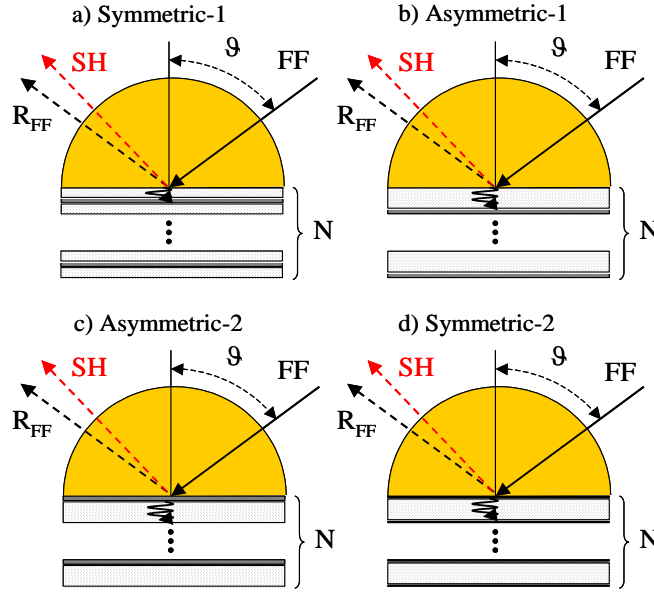
$$\eta = S_z^{SH} / S_{z,inc}^{FF}.$$


Fig. 1. Scheme of the configurations studied: a hemi-cylindrical prism that acts as input medium, on which a periodic metal/dielectric multilayer is grown. The output medium is air. (a) The elementary cell is symmetric (MgF₂/Ag/MgF₂). (b) The elementary cell is asymmetric (MgF₂/Ag). (c) The elementary cell is asymmetric (Ag/MgF₂/Ag). (d) The elementary cell is symmetric (Ag/MgF₂/Ag). The SHG is studied for a pump field tuned at 800nm and the SH generated at 400nm. The prism is made of fused silica whose refractive indices at 800nm and 400nm are respectively $n_{in}(800\text{nm}) = 1.53837$ and $n_{in}(400\text{nm}) = 1.55774$. The refractive indices of Ag and MgF₂ are respectively, $n_{Ag}(800\text{nm}) = 0.144 + 5.289i$, $n_{Ag}(400\text{nm}) = 0.173 + 1.95i$, $n_{MgF_2}(800\text{nm}) = 1.3751$, $n_{MgF_2}(400\text{nm}) = 1.3839 + 0.02i$. In the figures are also represented the input fundamental frequency (FF) pump field and the reflected FF and SH fields.

Before closing this Section we would like to underline that our description of the quadratic nonlinearities of metals in terms of a volume nonlinearity and a surface nonlinearity, which basically follows the classical approach outlined in the book of Shen [3], it is not the only method present in literature. At this regard it is worthwhile to mention the so-called hydrodynamical model [22] which is based on the hydrodynamic theory of the electron gas of the metals and even recently it has been the subject of extensive investigations [23]. Here we chose the classical model outlined in Ref. [3, 19] because of its much simpler numerical implementation and because we have already successfully used it to describe the experimental results on SHG in the non-plasmonic regime reported in Ref. [19]. In the next Sections we discuss the results obtained for the SH conversion efficiencies in the plasmonic regime.

3. Results and discussion

We have performed a systematic study of the SH generated at $\lambda = 400\text{nm}$ as a function of: a) the angle of incidence (θ) of the FF pump field at $\lambda = 800\text{nm}$; b) the thickness of the metal (d_{Ag}), and the dielectric (d_{MgF_2}) layers; c) the number of elementary cells (N). The variation of the angle of incidence has been limited to the total internal reflection regime, i.e. $90^\circ > \theta > \arcsin(n_{\text{out}}/n_{\text{in}})$ which in our case corresponds to $90^\circ > \theta > 40.8^\circ$. To compare more easily the behavior of the different elementary cells, d_{Ag} and d_{MgF_2} refer, respectively, to the total amount of silver and of magnesium-fluoride inside the elementary cell. Moreover, the thickness of the magnesium-fluoride layers has been limited to value below 600nm and above 10nm , while the thickness of the silver layers has been limited to values not exceeding 180nm and not less than 9nm . Note that a $9\text{-}10\text{nm}$ layer is currently at the boundary of sputtering or evaporation growing techniques. Moreover, and more importantly, for silver layers much thinner than 10nm , the classical description of the metals might be hampered by the insurgency of quantum-size effects [24]. As we will see later, for some configurations a maximum of the conversion efficiency has been predicted when the thickness of the constituent materials reaches their extreme values. These cases will be discussed later on in the text. All the conversion efficiencies refer to an intensity of the incident FF pump field of 6 GW/cm^2 which can be readily achieved by focusing on the sample the light coming from a Ti-sapphire laser [19], for example. In the calculations we have not included the transmission coefficient at the air/prism interface.

In order to better understand the main mechanisms that bring to an efficient SH generation, and to clarify how the different terminations of the elementary cell affect the nonlinear process, we will start our analysis by studying SH generation as a function of d_{Ag} and θ , when the thickness of the dielectric material is kept fixed to its maximum value of 600nm and the structures consist of only one period. The results are reported in Fig. 2 for the four kinds of elementary cells. While here we will show the figures only for the case with the total thickness of the dielectric material kept fixed at 600nm , we have also uploaded multimedia material with animations that show how the conversion efficiency changes by changing the thickness of the dielectric material for the four elementary cells under consideration (see multimedia [Media 1](#), [Media 2](#), [Media 3](#), [Media 4](#)).

Let us start by commenting Fig. 2(a) which refers to the Symmetric-1 elementary cell. For this elementary cell the layer of silver is surrounded by MgF_2 ; when d_{MgF_2} is very thick this configuration mimics the situation of a single layer of silver embedded in MgF_2 (the dielectric acts as input and output medium). In a pure $\text{MgF}_2/\text{Ag}/\text{MgF}_2$ structure, when the field is evanescent in MgF_2 and the thickness of the metal is thick enough, uncoupled surface plasmons can be excited at both metal/dielectric interfaces. These modes follow the classical plasmon dispersion relation at a metal/dielectric interface [25]:

$$k_{sp} = k_0 \sqrt{\frac{\epsilon_1 \epsilon_2}{\epsilon_1 + \epsilon_2}}, \quad (2)$$

where ϵ_1 and ϵ_2 are the dielectric permittivity of the two materials. In our case from Eq. (2) we find a value of the plasmon k -vector that corresponds to an incident angle of $\sim 67.7^\circ$ in fused silica (our input medium). As it is well-known [26], in general, when the thickness of silver decreases, the two surface plasmons can couple and generate two new kinds of plasmonic modes: the long range and the short range plasmons [26]. In Fig. 2(a) the black dashed lines represent the dispersion of the short-range/long range plasmon as calculated for a $\text{MgF}_2/\text{Ag}/\text{MgF}_2$ structure with MgF_2 as input and output medium. The dispersion of the short-range/long-range plasmon is calculated according to the recipe laid out in Ref. [27], using the transmission function of the structure. We can see from Fig. 2(a) that the peak of SH conversion efficiency of our true structure ($\text{SiO}_2/\text{MgF}_2/\text{Ag}/\text{MgF}_2/\text{air}$) follows closely the dispersion of the long/short range plasmon of the $\text{MgF}_2/\text{Ag}/\text{MgF}_2$ structure. We now note that the dispersion of a true long range plasmon is confined between 63.5° and 67.7° . As it must be

because for $\theta < 63.5^\circ$ the fields propagate in MgF_2 and plasmon modes are forbidden. On the other hand, we note that for our structure ($\text{SiO}_2/\text{MgF}_2/\text{Ag}/\text{MgF}_2/\text{air}$) the region of high SH conversion efficiency extends below $\theta = 63.5^\circ$. Here it comes into play the explanation we have anticipated at the beginning of the previous section: the long range plasmon typical of the $\text{MgF}_2/\text{Ag}/\text{MgF}_2$ structure gradually changes into a leaky waveguide mode of the $\text{SiO}_2/\text{MgF}_2/\text{Ag}/\text{MgF}_2/\text{air}$ structure. At this regard it must be noted that long range plasmons are characterized by a deeper penetration length in the surrounding dielectric, so they are more likely to feel the perturbation introduced by the actual structure. As these leaky waveguide modes are the natural evolution of long range plasmons, we will still refer to the associated enhanced SH generation as due to long range plasmons. We instead refer to the enhanced SH generation due to leaky waveguide modes for the cases when these modes are not the natural prosecution of the long range plasmons.

We now go to analyze the asymmetric-1 elementary cell reported in Fig. 2(b). For large values of d_{Ag} and d_{MgF_2} it can be assimilated to a MgF_2/Ag interface, with plasmon excitation at 67.7° ; and in fact that resonance is clearly visible in the figure. On the other hand, for thin silver thicknesses the field can reach also the interface with air so that a surface plasmon at the Ag/Air interface can be excited at an angle of 41.45° in fused silica for the FF and at an angle of 48.84° at the SH. Both resonances are visible in the figure, even though the 48.84° resonance is very weak.

The Asymmetric-2 elementary cell is specular to the Asymmetric-1, although the 1 period Asymmetric-2 structure supports only the Ag/MgF_2 interface plasmon. From Fig. 2(c) we can see two distinctive resonances: one resonance is, of course, the single interface plasmon, the second corresponds to the excitation of a leaky mode in MgF_2 . In fact, if we change the thickness of MgF_2 [see Media 3] from 50nm to 600nm in steps of 50nm, we see that for $d_{\text{MgF}_2} = 50\text{nm}$ there are two resonances: one weak at 67.7° and one strong at 50° . As d_{MgF_2} grows, the strong resonance move towards the weak until they merge, meanwhile another resonance appears and starts to moves toward the 67.7° . If we let the thickness of MgF_2 keep growing (not shown in the multimedia), this new resonance reaches a saturation value below 67.7° and other resonances start to appear. The appearance of new resonances as the thickness of the dielectric material increases should not be too surprising after all: this is what normally happens also in conventional dielectric waveguides that admit more and more guided modes for increasing values of the core thickness.

Lastly we consider the 1period Symmetric-2 structure studied in Fig. 2(d). In this case there are three interfaces that can support plasmonic modes: two MgF_2/Ag interfaces, and one Ag/air interface. The Ag/Air plasmon resonance at 41.45° is clearly visible in the figure. The two Ag/MgF_2 plasmons couple as in a metal/dielectric/metal waveguide and generate the two resonances around 67.7° . This behavior is confirmed by Media 4, in which it is possible to see how the two resonances tend to collapse as the thickness of the dielectric increases degenerating into the single surface plasmon resonance at 67.7° . At this regard we note that in both Symmetric-1 and Asymmetric-1 configuration it is the dielectric to be attached to the prism. This allows both structures to efficiently generate SH also for thick layers of metal. On the other hand, in the Asymmetric-2 and in the Symmetric-2 it is the metal in direct contact with the prism. In this second case, the field must reach the second Ag interface in order to produce a relevant conversion efficiency meaning that only structures with thin layers of silver will be efficient.

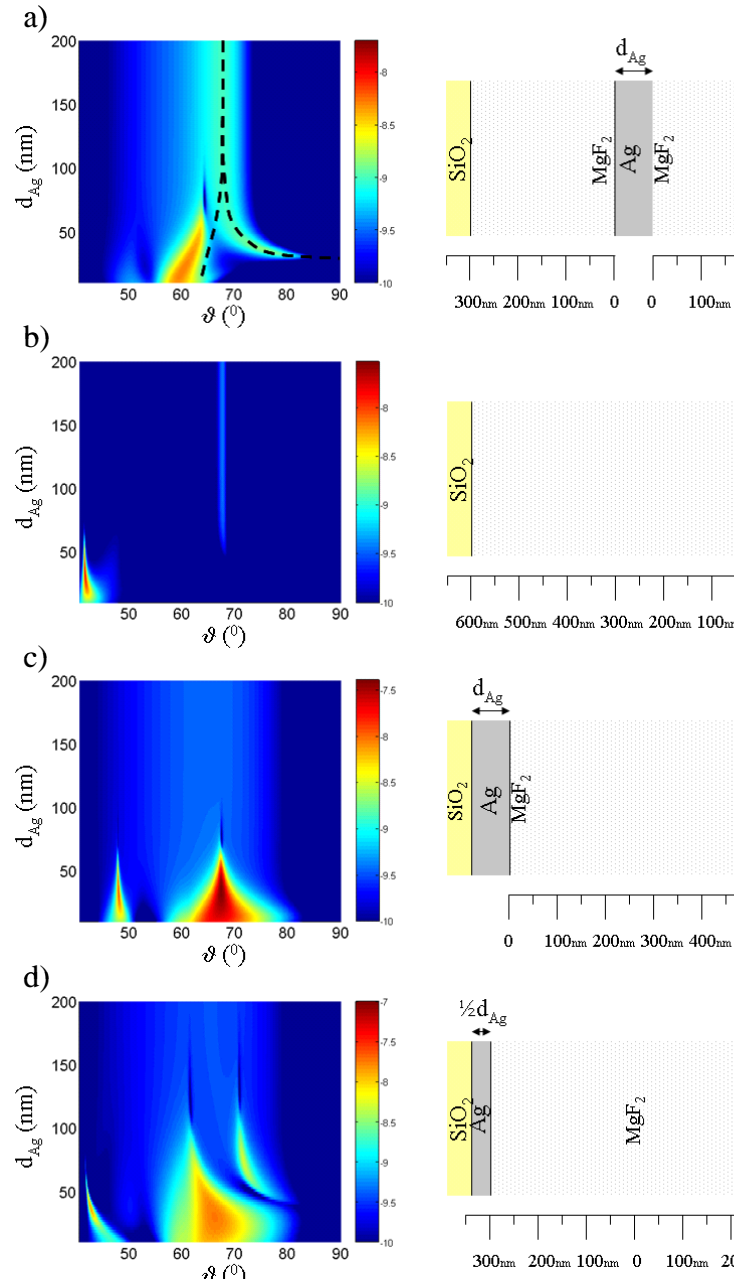


Fig. 2. Left side: $\text{Log}(\eta)$ vs. Ag thickness and incident angle for the 1-period structures considered, η is the conversion efficiency. Right side: Schematic representation of the structures considered: Symmetric-1 (2a), Asymmetric-1 (2b), Asymmetric-2 (2c), Symmetric-2 (2d). In Fig. 2(a) the black dashed line superimposed represents the dispersion of the short-range/long-range plasmons for the structure MgF₂/Ag/MgF₂. For each figure, see also the multimedia material ([Media 1](#), [Media 2](#), [Media 3](#), and [Media 4](#)) where the thickness of the MgF₂ is varied.

Moreover, we note that only the asymmetric-1 and the symmetric-2 structures exhibit a silver/air interface. Therefore, only those structures can support Ag/air interface plasmons.

In Fig. 3 we show topographic views arranged in a table environment of the maximum conversion efficiency as function of the thickness of the layers; then, in Fig. 4 we show, in a similar way, the angle at which that conversion efficiency is reached. Basically each plot corresponds to the maximum conversion efficiency for a given number N of elementary cell and a given type of elementary cell. Each point of the plot corresponds to a different value of the angle of incidence. Once the type of elementary cell and the number of periods are fixed, the conversion efficiency becomes a function of the angle of incidence and the thickness of the layers. In Fig. 3, d_{Ag} and d_{MgF_2} are the variables; this means that the conversion efficiency is still dependent upon a parameter: the angle of incidence. This parameter is chosen point by point in order to maximize the conversion efficiency and its value is reported in Fig. 4. The intensity scale of each conversion efficiency plot (Fig. 4) is logarithmic and runs from 10^{-10} (dark blue, which means value of the conversion efficiency $\leq 10^{-10}$) up to maximum value of $3 \cdot 10^{-7}$ (dark red). The intensity scale of each angle (Fig. 4) is linear and runs from 40.8° (total internal reflection at SiO_2/Air interface) up to 90° .

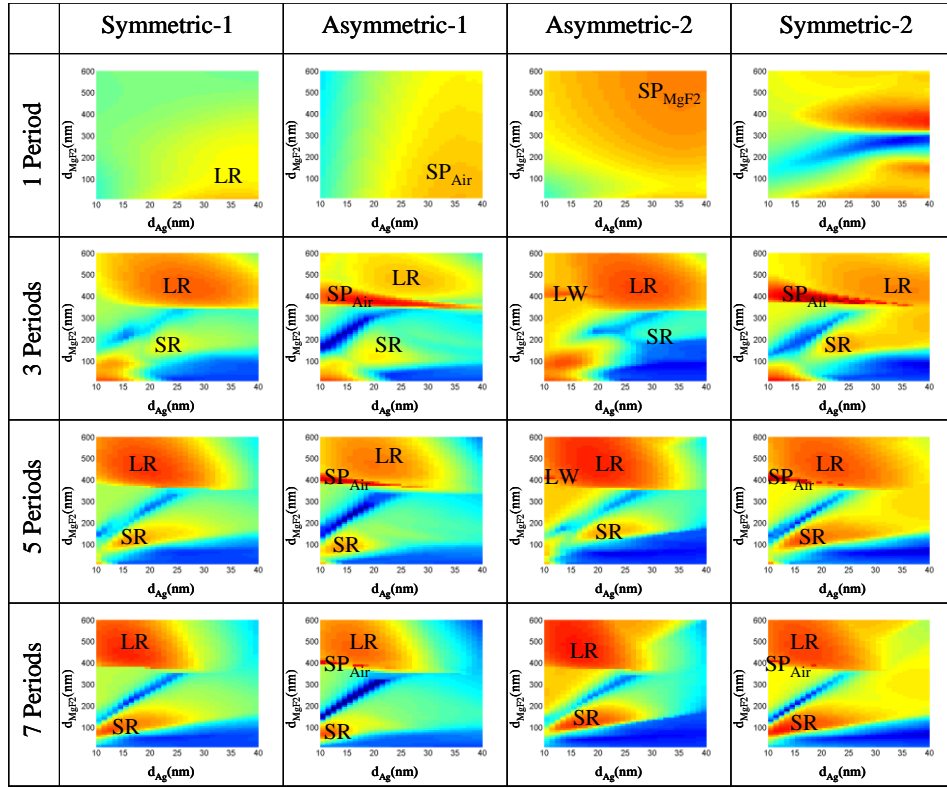


Fig. 3. Maximum conversion efficiency accessible as function of the thickness of the layers for a given number and a given type of elementary cell. Superimposed an acronym that indicates the type of resonant mechanism: LR indicates that the enhanced SH generation is due to the excitation of long range plasmons; SR indicates that the enhanced SH generation is due to the excitation of short range plasmons; SP_{Air} indicates that the enhanced SH generation is due to the excitation of a plasmon at the Ag/Air interface; SP_{MgF_2} indicates that the enhanced SH generation is due to the excitation of a plasmon at the Ag/MgF₂ interface; LW indicates that the enhanced SH generation is due to the excitation of a leaky waveguide mode.

First of all we note that the conversion efficiency can be up to three orders of magnitude greater than the conversion efficiency experimentally found and theoretically predicted in Ref. [19] in the non-plasmonic regime. Moreover, with our choice of parameters, a classical Kretschmann geometry having air as output medium (like the one analyzed in Ref. [4].) will generate SH with a peak efficiency of $5.56 \cdot 10^{-8}$, which is one order of magnitude lower than

the one that is possible to achieve with a periodic structure. Second, for a large number of periods all the structures seem to converge to approximately the same conversion efficiency, while major differences can be found for few repetitions of the elementary cell. We must emphasize that for $N > 3$ the structures are almost identical and differ by their end faces only. This is why the SH generation for the various structures tends to converge for increasing number of periods.

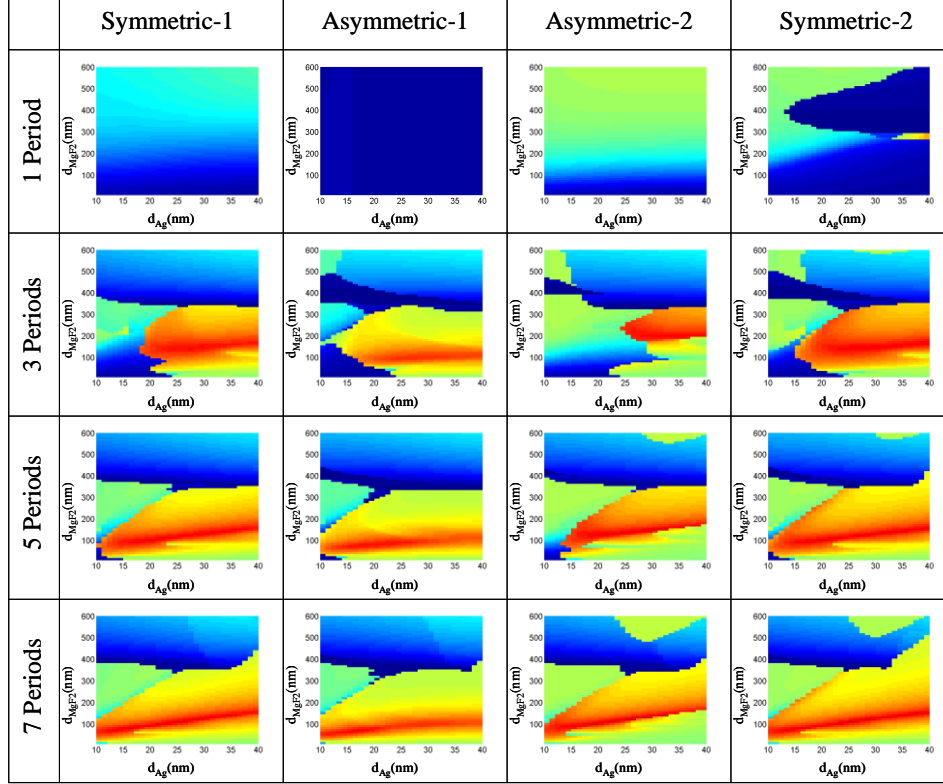


Fig. 4. Angle at which the conversion efficiency reported in Fig. 3 is reached as a function of the thickness of the layers for a given number of periods and a given type of elementary cell.

When more periods are added, all the structures will have at least one silver layer embedded in MgF_2 . Therefore, long range and short range plasmons can be excited for all structures when the number of periods is greater than one and for the symmetric-1 structure regardless of the number of periods. Moreover, the short/long range plasmons will split accordingly to the number of silver layers fully embedded in MgF_2 . Due to high penetration length of the long range plasmon in MgF_2 , long range resonances will be dominant for relatively large thickness of MgF_2 and will be excited for a wide range of angle around 60° ($50^\circ \leq \theta \leq 70^\circ$). When d_{MgF_2} decreases, the long range plasmons gradually lose their plasmonic character, meanwhile the conversion efficiency drops. On the other hand, short range plasmons will be advantaged by the use of thinner dielectric layers because of their short penetration length inside the dielectric surrounding the metal. For a small number of periods, other resonances related to the specific termination of the elementary cell can appear. In particular the asymmetric-1 and the symmetric-2 support also a plasmon excitation at the Ag/air interface ($\theta \approx 41.45^\circ$), while the asymmetric-2 supports leaky waveguide modes. As a matter of fact, the enhanced SH conversion efficiency associated with these resonances tends to be wiped out as the number of periods increase. We also note that all the structures should support a resonance in correspondence to the excitation of a plasmon at a single Ag/ MgF_2 interface ($\theta \approx 67.7^\circ$). In order to access this resonance a large value of silver thickness

($d_{Ag} > \sim 60\text{nm}$) is required for the symmetric-1 and the asymmetric-1 structures so that the plasmon created at the first MgF_2 interface is isolated (note that d_{Ag} will be out of the scale of Fig. 3 and Fig. 4), while a large thickness of MgF_2 is necessary for the asymmetric-2 and the symmetric-2 structures, so that the plasmon excited at first Ag/MgF_2 interface is isolated.

We can see from Fig. 3 that the SH resonance associated with short range plasmons requires thinner thicknesses of the constituent materials as the number of periods increases. A similar behavior can be also noted for the long range plasmons: the peak area shrinks on the d_{Ag} scale as the number of periods increases. This phenomenon can be explained in the framework of plasmons tunneling: for structures with a large number of periods shorter thicknesses are required in order to allow an efficient coupling of the plasmons excited at each metal/dielectric interface.

From Fig. 3 we can see that the maximum of the conversion efficiency for the 1 period Asymmetric-2 structure is out of the range considered for the MgF_2 layers thickness. Therefore, these maxima of the conversion efficiency appear in a geometry in which MgF_2 can be considered as a semi-infinite medium. This result indicates that high conversion efficiencies can probably be obtained in a standard Kretschmann geometry by simply changing the output medium. To the authors' knowledge, up to now, in Kretschmann geometry, the output medium has always been assumed to be air. We will return later on this interesting aspect. Lastly, we note that when the ratio of the dielectric layer to the metallic layer is about 15 ($d_{\text{MgF}_2}/d_{Ag} \sim 15$) all the structures show an anti-resonant behavior and it is not possible to efficiently generate SH.

Many factors determine the performance of SH generation in multilayered structures, among them the most important are the field localization at the FF and at the SH and the phase matching conditions [19, 28]. In our case the field localization is associated with the plasmon excitation. High SHG generation is reached when there is high field localization both at the FF and at the SH (i.e. the respective plasmon dispersion curves must somehow overlap) and when there is the right interference between these fields (phase matching condition).

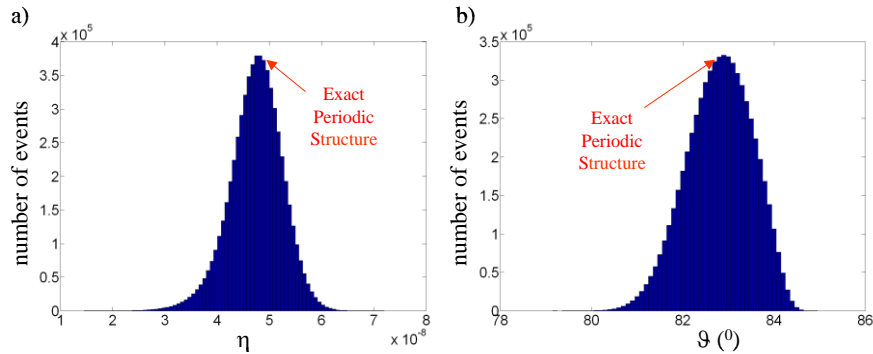


Fig. 5. (a) Histogram of the conversion efficiency and (b) angle at which it is obtained when each layer is randomly varied around its central value according to a Gaussian distribution having a standard deviation from the central value equal to 5%. The structure considered is N=5-periods Symmetric-1 for which the maximum conversion efficiency of $\eta=4.9 \times 10^{-8}$ is reached when $d_{Ag}=15\text{nm}$ and $d_{\text{MgF}_2}=101\text{nm}$ which represent our central values in the statistical study. The histograms have been obtained after 6318856 simulations.

In order to check the robustness of SH generation against possible errors in the fabrication of an actual sample, in Figs. 5(a) and 5(b) we present a statistical analysis of the N = 5-periods Symmetric-1 type structure. In particular, in Figs. 5(a) and 5(b) are reported two histograms: Fig. 5(a) is relative to the maximum conversion efficiency while Fig. 5(b) is relative to the angle at which the maximum conversion efficiency is obtained. Each layer is randomly varied according to a Gaussian distribution centered on the short range resonance as indicated in Fig. 3, and having a standard deviation equal to 5% of the central value. The histograms have been obtained after 6318856 simulations. We note that the conversion efficiency of the ideal

structure is in the middle of the histogram. This means that on one hand the structure is stable and, on the other hand, the periodic structure it is not the most efficient structure and therefore an optimized device for efficient plasmonic SHG might eventually pass through the study of more sophisticated, non-periodic geometries.

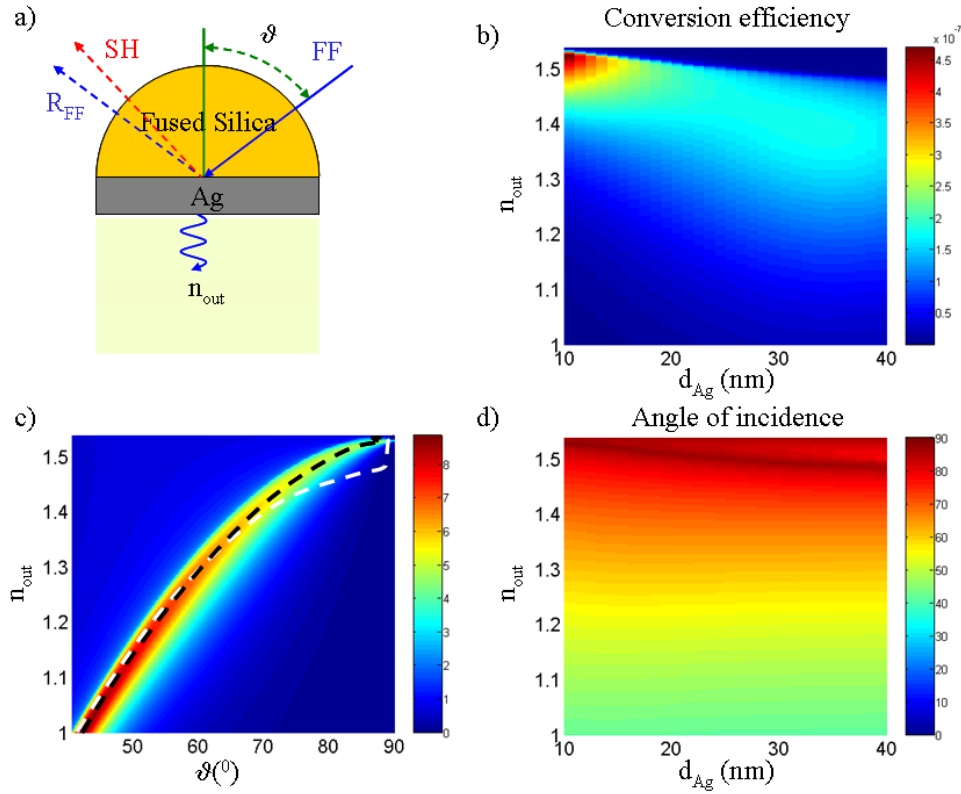


Fig. 6. (a) Classical Kretschmann geometry where the input medium is a fused silica prism, the metal is silver, and the output medium is a generic non absorptive non dispersive dielectric of index of refraction n_{out} . (b) Maximum conversion efficiency achievable vs. the Ag layer thickness and the index of refraction of the output medium (n_{out}). (c) Transmission as a function of the angle of incidence and of n_{out} when $d_{Ag} = 10\text{nm}$. The transmission maxima correspond to the dispersion of the leaky wave in the fused silica. The white dashed line is the dispersion of the surface plasmon at the Ag/ n_{out} interface calculated according to the standard dispersion law: $k_{SP} = k_0 \sqrt{\epsilon_{Ag} \epsilon_{out} / (\epsilon_{Ag} + \epsilon_{out})}$. The black dashed line represents instead the loci of the maxima of the SHG. Note how the loci of the maxima of the SHG follow exactly the dispersion of the leaky wave. Note also as the dispersion of the Ag/ n_{out} surface plasmon is similar to the dispersion of the leaky wave. (d) Angle at which the maximum conversion efficiency is obtained vs. d_{Ag} and n_{out} .

Before going to the concluding remarks, we would like finally to discuss the fact that in this paper we have restricted our study to plasmonic structures in which the output medium is air. We have found that a properly designed structure can have a conversion efficiency $\eta \sim 3 \times 10^{-7}$ for $\sim 6\text{GW/cm}^2$ pump intensity. This value of the conversion efficiency was obtained by using just the metal surface nonlinearities that are naturally included in any metallo-dielectric filter. Now, if we had carefully chosen the material of the output medium there would have been even further room for strong improvements. To this end, in Fig. 6(b) we show SH generation in a classical Kretschmann configuration, see the scheme reported in Fig. 6(a), as a function of the Ag thickness and of the refractive index of the output medium. The figure shows that by considering an output medium of refractive index $n \sim 1.4$ and a single layer of Ag approximately $\sim 40\text{nm}$, conversion efficiency of $\eta \sim 2 \times 10^{-7}$ (i.e. of the same order

of that previously found in more complicate structures) is readily achievable. By further increasing the refractive index of the output medium to arrive around $n \sim 1.5$ we obtain a conversion efficiency $\eta \sim 4 \cdot 10^{-7}$. However, note from Fig. 6(d) that this high conversion efficiency is reached when the angle of incidence is grazing.

As we will see in a moment, the peak of the conversion efficiency in this geometry is linked to the excitation of leaky surface waves that mimic the surface plasmon at the Ag/n_{out} interface. First we note that in this case the silver layer is placed in an asymmetric environment ($n_{\text{in}} \neq n_{\text{out}}$). We know from the work of Ref. [29], that in general a thin metal layer in an asymmetric environment may admit four modes, two bound modes and two leaky modes. In particular, the two leaky modes show localization at the metal dielectric interface Ag/n_{in} (Ag/n_{out}) very similar to a standard surface plasmon, while they couple to radiation fields, i.e. they leak energy, in the medium n_{out} (n_{in}) [29]. In the case of our configuration, simple considerations about transverse momentum conservation can show that the only mode compatible with the transverse momentum conservation of the incident field is the one that leaks in the input medium (fused silica) and it is localized like a surface plasmon at the Ag/n_{out} interface. This leaky wave is the one responsible for the enhancement of the SH as we show in Fig. 6(c) where we have reported the dispersion of the leaky wave in the fused silica and superimposed the loci of the maximum SHG (black-dashed line) in the case of a 10nm Ag layer. Once more, we point out that the dispersion of the leaky wave has been calculated by using the transmission function of the structure according to the recipe laid out in Ref. [27]. As the reader can easily ascertain, the loci of the maxima of the SHG follow exactly the dispersion of the leaky wave in the fused silica. For the benefit of the reader, we have also reported in Fig. 6(c) the dispersion of the surface plasmon at the Ag/n_{out} (white dashed line) to confirm its close similarity with the dispersion of the leaky wave in agreement with the results reported in Ref. [29].

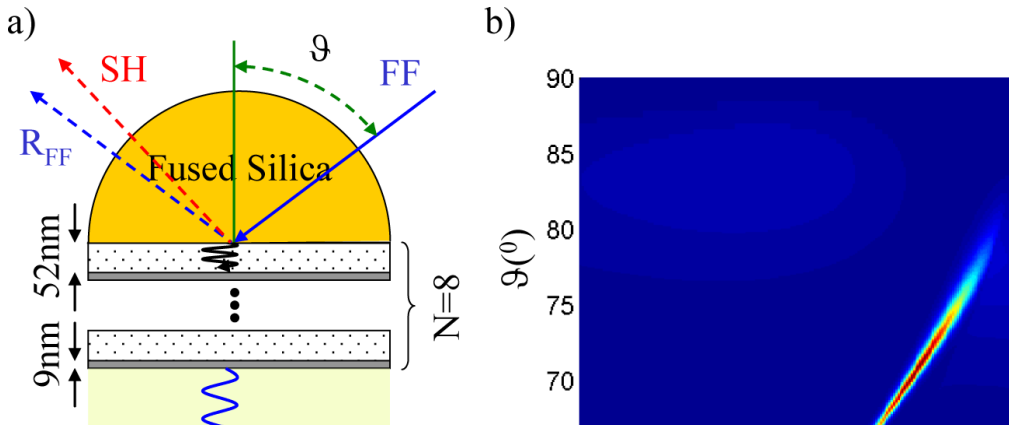


Fig. 7. (a) Scheme of the configuration studied. The 8-periods asymmetric-1 structure with $d_{\text{Ag}}=9\text{nm}$ and $d_{\text{MgF}_2}=52\text{nm}$ is grown on the base of a fused silica hemi-cylindrical prism, while the output medium is a generic non absorptive non dispersive dielectric of index of refraction n_{out} . (b) Conversion efficiency vs. the index of refraction of the output medium (n_{out}) and the angle of incidence θ .

In Fig. 6(d) we finally show the angle at which the maximum SH conversion efficiency is achieved as function of the thickness of the Ag layer and the refractive index of the output medium. The figure shows that the maximum generation is independent from the Ag thickness, a fact that reinforces the notion that the enhanced SH is due to a surface-plasmon-like mode. In view of the above considerations we may say that a careful optimization of a metallo-dielectric multi-layered structure which includes the optimization of the output medium might reasonably bring an additional enhancement in the conversion efficiency by two or three orders of magnitude. As an example, we consider an 8-periods asymmetric-1 structure. For $d_{\text{Ag}} = 9\text{nm}$, $d_{\text{MgF}_2} = 52\text{nm}$ and at an angle of incidence of 83.2° , a SH resonance

$\eta \sim 1.2 \times 10^{-7}$ associated with short range plasmon excitation is found. We now calculate the conversion efficiency for the optimized structure, which is schematically represented in Fig. 7(a), as a function of the angle of incidence and of the refractive index of the output medium. The results are reported in Fig. 7(b). According to our calculations the conversion efficiency improves by an additional factor of 20 when the refractive index of the output medium is around 1.4.

4. Conclusions

In this paper we have studied SH generation from periodic metallo/dielectric stratifications in the plasmonic regime. The conversion efficiency is estimated to be some four to five orders of magnitude higher than the conversion efficiency experimentally found and theoretically predicted in the non-plasmonic regime [19]. We have clarified the role played in the SHG process by the single interface surface plasmons, by the short-range/long-range plasmons at the double interface and by the leaky waves. We have also pointed out that there are still vast margins of improvement by considering more sophisticated, non-periodic structures and by carefully choosing the output medium. The subject of SHG in the plasmonic regime remains still today a vital field of research which we believe has many pleasant surprises yet to reveal.

Acknowledgments

We thank M. Scalora for helpful discussions. This work is supported by Defense Advanced Research Projects Agency (DARPA) project W31P4Q-09-C-0347 "Nonlinear Plasmonic Devices".